Bulgarian Chemical Communications, Volume 52, Special Issue E (pp. 88 - 92) 2020

Impedance spectroscopy studies of the electrochemical hybrid supercapacitors based on activated carbon and iron oxides

Elefteria Lefterova*, Svetlana Veleva, Antonia Stoyanova

Acad. Evgeni Budevsk Institute of Electrochemistry and Energy Systems - Bulgarian Academy of Sciences, Akad. G. Bonchev 10, 1113 Sofia, Bulgaria

Received February 10, 2020; Accepted April 17, 2020

Symmetric and hybrid supercapacitors were developed and investigated by electrochemical impedance spectroscopy (EIS). Activated nanoporous carbon (commercial product, TDA Research, USA) and electrochemically active iron oxides - Fe_2O_3 (hematite) and Fe_3O_4 (magnetite) were laboratory synthesized and used as electrode materials for assembling of supercapacitor cells. $LiBF_4$ with an organic solvent mixture of ethylene carbonate/dimethyl carbonate (1:1) was served as an electrolyte. The results from EIS measurements show the possibility of application of magnetite and hematite as electrochemically active materials for hybrid lithium battery–supercapacitor systems and can provide guidance in selection the most suitable metal oxides, as composite electrode materials in supercapacitors.

Keywords: Magnetite, hematite, activated carbon, hybrid supercapacitors, impedance spectroscopy

INTRODUCTION

Among the various advanced solutions, concerning energy storage and conversion technologies, energy can in particular be stored electrochemically in accumulators (batteries) and supercapacitors (SCs). Although batteries currently present much higher energy density, their relatively low power density and poor cycle life hinder high power demanding applications such as regenerative braking systems. By contrast, supercapacitors store larger amounts of energy than the traditional dielectric capacitors and provide energy far faster than batteries. Therefore, they are particularly adapted for applications requiring energy pulses in short periods of time [1]. Although supercapacitors are now commercially available, they still require improvements, especially for enhancing their energy density and cut the cost at the same time. Hybrid electrochemical systems involving hybridization of a faradaically rechargeable battery-type electrode with an electrochemical double-layer capacitor-type electrode (e.g. asymmetric supercapacitors) show promising capability to achieve this [2]. On this basis various hybrid capacitor configurations, consisting of activated carbon and a negative electrode based on metal oxides (nickel, lead or manganese oxides) in non-aqueous electrolytes, are studied [2, 3].

The iron oxides - Fe_2O_3 and Fe_3O_4 are promising electrode materials for lithium-ion batteries because of their low cost, simple manufacturing process, wide range of sources, non-toxicity and environmental friendliness, and mainly – large theoretical specific capacity of both oxides [4-6].

In our previous studies hybrid lithium battery-supercapacitors are assembled by an electrode of activated carbon, a composite electrode with activated carbon matrix and addition of 50 wt. % Fe_3O_4 or Fe_2O_3 and they are subjected to charge/discharge cycling test under galvanostatic conditions at different current loads and continuous cycling. It is found, that the developed hybrid supercapacitors, especially the magnetite based cell, demonstrate high current efficiency and specific capacity higher than the capacities of the basic symmetric capacitor as well as stable capacity behaviours at prolong cycling [7].

These results prove the possibility of application of magnetite and hematite as electrochemically active material for hybrid lithium battery–supercapacitor systems and provoked our further interest in detailed study of their electrochemical properties.

Usual testing schedule of SCs was always followed involving galvanostatic charging/discharging, cyclic voltammetry and other recommended experiments. The electrochemical impedance spectroscopy (EIS) of supercapacitors provide additional information about the faradaicreactions, internal resistances as serial resistance and charge transfer resistance.The advantage of the EIS over other testing techniques of SCs is the possibility of identification, separation and evaluation of the characteristic resistances as

* To whom all correspondence should be sent.
E-mail: e.lefterova@iees.bas.bg

electronic contacts at the current collector/ active electrode interface, charge transfer, electric resistance of the electrode, diffusion, etc . In addition, the pseudocapacitance of the electrode can be distinguished from the double-layer capacitance over a range of frequencies [8].

The objective of the present work is to investigate using impedance spectroscopy an electrochemical hybrid lithium battery-supercapacitor composed by an activated carbon electrode, a composite electrode with activated carbon matrix and addition of Fe_2O_3 and Fe_3O_4, and a non-aqueous electrolyte.The results obtained from EIS can be used as guidance in selecting the most suitable metal oxides as electrode materials for supercapacitors.

EXPERIMENTAL

Synthesis of nanosized Fe_2O_3 and Fe_3O_4

Activated nanoporous carbon (AC) and electrochemically active iron oxides - α-Fe_2O_3 (hematite) and Fe_3O_4 (magnetite) were used as electrode materials for assembling of hybrid supercapacitor cells.

Nanosized magnetite and hematite were laboratory synthesized. Magnetite was obtained by sonochemical synthesis which is carried out by precipitation the corresponding metal hydroxides and their further decomposition to oxides under ultrasonic irradiation. As starting compounds $FeCl_2.6H_2O$, $Fe(NO_3)_3.9H_2O$ and NaOH in a molar ratio of 1:2:5 were used.

Hematite was obtained by solution combustion synthesis method. As starting reagents $Fe(NO_3)_3.9H_2O$ and sucrose (as fuel) in 3.2:1 molar ratio were used. Stoichiometric amounts of the reagents were dissolved in an appropriate amount of deionized water.

The activated carbon is a commercial product (TDA Research, USA).

Preparation of hybrid supercapacitor cells and electrochemical testing

The activated carbon and iron-oxides (Fe_2O_3 or Fe_3O_4) were used to fabricate electrodes for two types of electrochemical cells for capacity measurements. The first type is a symmetric supercapacitor cell using two identical electrodes from activated carbon and a non-aqueous electrolyte – lithium tetrafluoroborate ($LiBF_4$) with organic solvent – ethylene carbonate and dimethyl carbonate (EC/DMC) mixture in ratio 1:1. The second one was a hybrid battery - supercapacitor cell, which was assembled by a composite electrode and an activated carbon electrode. The composite (negative) electrode was prepared of activated carbon matrix with addition (50 wt. %) of iron oxide – Fe_2O_3 or Fe_3O_4. The positive electrode was made from the same activated carbon material. The same non-aqueous electrolyte – $LiBF_4$-EC/DMC (1:1) as in the symmetric supercapacitor cell is used. The prepared electrodes were soaked in organic electrolyte and then mounted in a coin-type cell with Glassmat separator andthe cell was filled with electrolyte.

Electrochemical impedance spectroscopy (EIS)

Electrochemical impedance spectroscopy (EIS) measurements were carried out, using Phase Sensitive Multimeters Newtons4th Ltd. PsimetriQ-PSM1700 equipped with Newtons4th Impedance Analysis Interface (IAI). Experiments were conducted in two electrode cell in frequency range of 1 MHz to 1 mHz with sampling rate of 10 points per decade, and A.C. sinusoidal amplitude 10 mV. All EIS experiments were performed after the 50th cycle to be sure that the formation of SEI is completed. EIS data were analyzed in terms of an equivalent circuit model and a complex non-linear least squares fitting (CNLS) algorithm was used.

Theoretical remarks

Electrical impedance was defined by applying an A.C. potential to an electrochemical cell and then measuring the current through the cell. The electric potential is $\Delta E(\omega) = E_o e^{i\omega t}$ with small E_o amplitude (5–10 mV) and an angular frequency $\omega = 2\pi f$. Responding current was determined by $\Delta I(\omega) = I_o e^{i\omega t+\varphi}$, where I_o is the current amplitude and φ is the frequency-dependent phase angle between the applied potential $\Delta E(\omega)$ and the measured current$\Delta I(\omega)$. Therefore, the impedance Z is defined as:

$$Z(\omega) = \frac{\Delta E(\omega)}{\Delta I(\omega)} = \frac{E_o e^{i\omega t}}{I_o e^{i(\omega t+\varphi)}} = \frac{E_o}{I_o} e^{-i\varphi} = |Z(\omega)|e^{-i\varphi} = Z'(\omega) + iZ"(\omega), \quad (1)$$

where Z'(ω) and $Z"$(ω) are the real and imaginary parts of the complex impedance respectively, and $|Z(\omega)|$ is a module as $|Z(\omega)|^2 = Z'^2 + Z"^2$ [9,10].

The complex capacitance $C(\omega) = C'^{(\omega)} - iC"(\omega)$ can be calculated from impedance data using equations [10]:

$$Z(\omega) = \frac{-1}{i\omega C(\omega)} \quad (2)$$

$$C'(\omega) = \frac{-Z"(\omega)}{\omega|Z(\omega)|^2} \quad (3)$$

$$C"(\omega) = \frac{Z'(\omega)}{\omega|Z(\omega)|^2} \quad (4)$$

In case of a pure capacitive behaviour (Z'=0 and C"=0, ideal capacitor) the relation is:

$$Z" = \frac{-1}{C\omega} \quad (5)$$

The plot of –Z'' versus 1/ω will be a straight line with a slope of 1/C and thus the capacity can be calculated [11].

The most used presentation of EIS data are Nyquist plot and Bode plot. In a complex plane (Nyquist plot) the real part is plotted on the X-axis and the imaginary part is plotted on the Y-axis. In Bode plot the impedance is plotted with log frequency on the X-axis and both the absolute values of the impedance |Z| and the phase-shift on the Y-axis. A typical Nyquist plot of an electrochemical supercapacitor is presented in Fig. 1. Four frequency bands are distinguished and each can be described with the corresponding elements. Therefore the capacitive electrochemical systems can be represented by connection of electrical elements in a suitable equivalent circuit. The semicircle at high to medium frequencies (2) describing with (RC) elements is due to pore resistance in EDLC, or charge transfer resistance in pseudo capacitors as well as to the electrical resistance of low conductive electrodes. The high frequency region (1), bounded by the beginning of the semicircle (left-intercept of Z'' at the Z' axis) gives the value of the effective series resistance (ESR) denoted as Rs and usually it is due to an electrical contact and/or electrolyte resistance. A line with slope ≅45° at medium frequencies (3) and a nearly vertical line at low frequencies describe the diffusion process and presents by Finite-Length Warburg element (FLW) with open reflective (blocking) terminus:

$$Z_D = R_D \frac{\coth(i\tau\omega)^{\frac{1}{2}}}{(i\tau\omega)^{\frac{1}{2}}} \qquad (6)$$

In the diffusion interpretation $\tau = L^2/D$ (L is the effective diffusion thickness, and D is the effective diffusion coefficient of the particle). At very low frequencies, the Z' approaches R and Z" continues to increase - similar to the behaviour of a capacitor. A Randles equivalent circuit was used to modelling such electrochemical cells with mixed kinetic and charge-transfer control (fig. 1c). At lack of homogeneity the semicircle is depressed and low frequency line is declined (red line, fig.1b). In this case a constant phase element **(**CPE) replaces the capacitor, and Generalized Finite Warburg element (GFW) replaces FLW in Randles equivalent circuit as:

$$Z_{CPE} = \frac{-1}{T(i\omega)^{\alpha}} \qquad (7)$$

$$Z_D = R_D \frac{\coth(i\tau\omega)^{\frac{\alpha}{2}}}{(i\tau\omega)^{\frac{\alpha}{2}}}, \qquad (8)$$

where T is a capacitive parameter (in $Fs^{\alpha-1}$), and α is the constant phase exponent ($0 \leq \alpha \leq 1$) reflecting the deviation from ideal case [9].

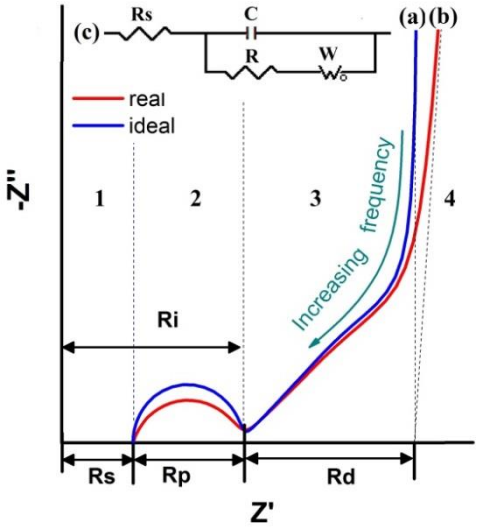

Fig. 1. Nyquist plot and equivalent (Randles) circuit model for the porous electrodes**.**

RESULTS AND DISCUSSION

Nyquist and Bode plots of the supercapacitors under investigation are shown in Figure 2 and Figure 3. The different electrochemical processes at the different frequencies ranges are well distinguished. The Nyquist plot of AC/AC and AC/AC+Fe_3O_4 are close. Their A.C. response is intrinsic to porous electrode and similar to the presented in fig. 1. The difference consists in the high to middle frequencies range (2) where instead of one, two overlapped semicircles are depicted as it is shown in the zoomed plot (Fig. 2b). For this reason, another RC element is added to the Randles circuit (fig. 4) and this equivalent circuit is used for fitting procedure. The results are presented in Table 1.

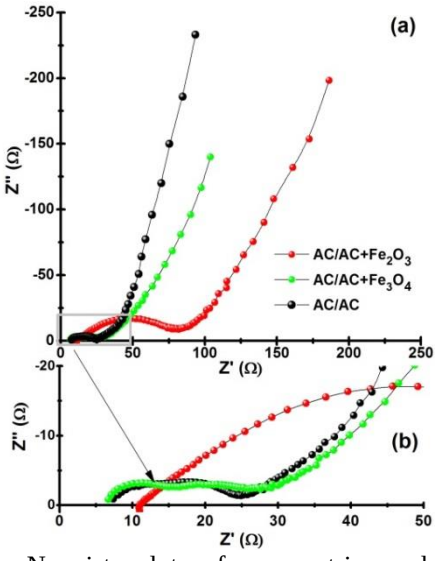

Fig. 2. Nuquist plot of symmetric and hybrid supercapacitors (a) full range; (b) the data of the high frequency range

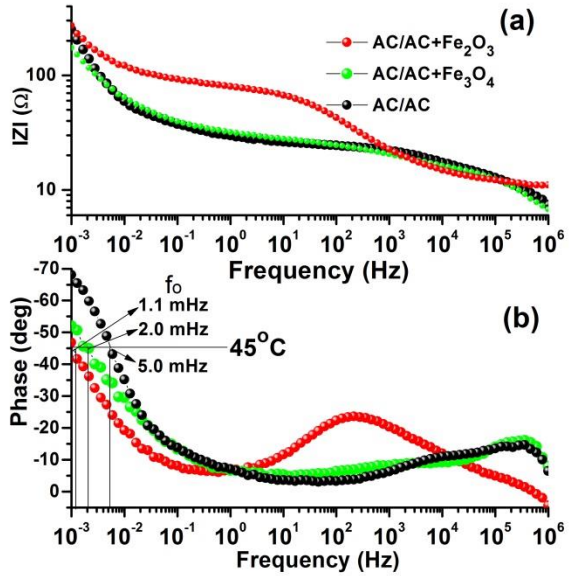

Fig. 3. Bode plots of symmetric and hybrid supercapacitors: (a) |Z| vs. frequency; (b) phase vs. Frequency

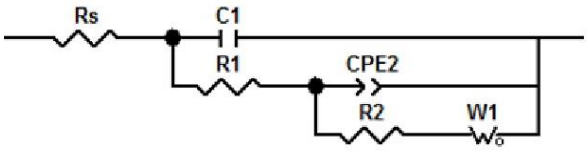

Fig. 4. Equivalent circuit describing EIS spectra

Different explanation of the high frequency semicircle exist in the literature as electronic resistance of the electrode, ionic resistance in the pores, charge transfer trough electrolyte-electrode interface etc.. Taking account very low capacitance (C1<1 μFcm^{-2}) this semicircle is due to ionic resistance in the pores. The second arc (frequency range 200 Hz-20 KHz) could be connected with lithium ion transport at separator interface or lithium ion (charge) transfer at an electrode/electrolyte interface (Rct) (at lower frequency) [12,13]. The weak broadening of the second semicircle of hybrid AC/AC+Fe_3O_4 cell is explained by the superposition of the two processes, one on the AC electrode and second of AC+ Fe_3O_4 electrode. For AC/AC+Fe_2O_3 cell a large depressed semicircle is visible. The internal resistance Ri of hematite electrode exceeds in times the internal resistance of the AC and AC+ Fe_3O_4 cells (Table 1) and it is related to the lower specific area in results of the larger particles size as well as the low conductivity of the hematite [7].

The Bode plot reveals that the reaction of the iron oxide contained electrodes are shifted to lower frequencies and therefore the processes are slower in the hybrid cells.

Table 1. Calculated impedance parameters

Cell	CLNS								Linear fit
	Rs	R1	C1	R2	CPE2 T	CPE	WR_D	χ^2	C
	Ω	Ω	μF	Ω	mFs$^{\alpha-1}$	α	Ω		F cm^{-2}
AC-AC	7.96	4.37	0.108	12.73	0.303	0.53	48.85	0.00027	0.707
AC-AC/Fe_3O_4	7.34	5.57	0.121	12.87	0.077	0.499	38.46	0.00124	0.961
AC-AC/Fe_2O_3	11.7	3	1.36	61.47	0.464	0.59	57.28	0.00041	1.333

The hybrid cells have a greater slope of the line at low frequency range. This non-ideality is a typical feature of electrochemical charging processes, and may be interpreted as resulting from a distribution in macroscopic path lengths (non-uniform active layer thickness) or a distribution in microscopic charge transfer rates [14], adsorption processes, or surface roughness as well as from diffusion restrictions. The diffusion character is maintained almost to 1 mHz for hematite electrode, as it can be seen from Bode plot and confirmed by characteristic frequency f_o (f_{oFe2O3}=1.1 mHz) (fig. 3b). Characteristic frequency f_o for capacitors is defined by the frequency where resistance and reactance are equal (-45°phase angle) i.e. f_o divided the frequency range in two: at $f<f_o$ capacitive (-90°≤phase<-45°) behaviour and at $f>f_o$ (-45°≤phase≤0°) resistive [15].

The Fig. 5 shows the frequency dependence of the real and imaginary parts of capacitance, calculated from equations (3) and (4). *C'* sharply increases, when the frequency decreases below 1 Hz. It tends to be less frequency dependent for AC/AC cell. The imaginary part of the AC/AC capacitance goes through a maximum at a frequency f_p =3.5 mHz defining a time constant τ_o (or relaxation time) as $\tau_o=1/f_p$ [10]. For the asymmetric cells $f_p \leq$ 1mHz, i.e. f_p is out of measured frequency range.

The plot of –Z" versus 1/f is a straight line at low frequencies as it can be seen from Figure 6. The capacitance of the cells was calculated from the slope according to equation (5).

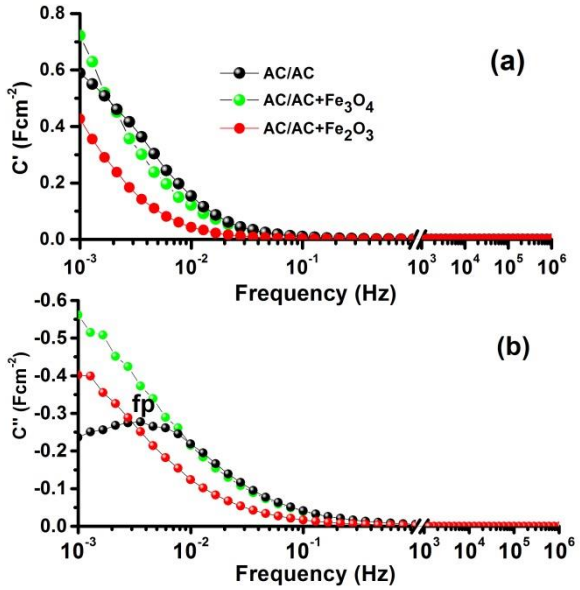

Fig. 5. Evolution of the real (C') and imaginary (C'') parts of capacitance *vs.*frequency

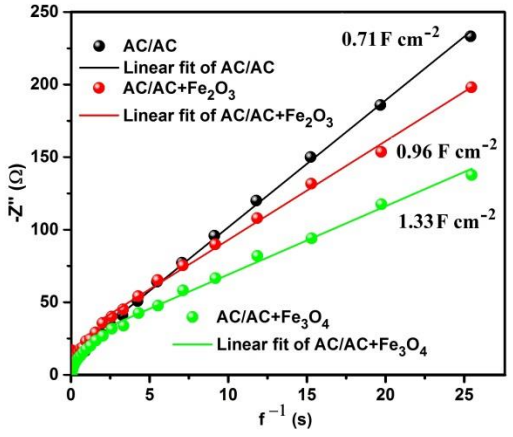

Fig. 6. The plot of the -Z'' vs. f^{-1}.

From CNLS and linear fit results summarized in Table 1, the following relationships are established: $R_s(AC/AC) \approx R_s(AC/AC+Fe_3O_4) < R_s(AC/AC+Fe_2O_3)$ and $R_2(AC/AC) \approx R_2(AC/AC+Fe_3O_4) < R_2(AC/AC+Fe_2O_3)$, where the higher $R_s(AC/AC+ Fe_2O_3)$ value is due to the higher resistance of the electrode caused by the lower electronic conductivity of the hematite. The highest capacitance is obtained for $AC/AC+Fe_3O_4$ cell. In spite the large resistance of the hematite electrode, this hybrid cell has relativelyhigh capacitance. This means that it is possible to significantly increase the hematite pseudo capacitance and reduce Ri, by increasing the specific surface area.

CONCLUSIONS

Electrochemical impedance spectroscopy (EIS) reveals that the magnetite based cell has the highest capacitance. In spite the highest intrinsic resistance the hematite electrode shows a relatively high capacitance, and hence possesses a potential for significantly increase of its pseudo-capacitance by optimizing the particle size and morphology. The results demonstrate the applicability of the EIS method for providing guidance on appropriate selection of metal oxides as composite electrode materials in supercapacitor systems.

Acknowledgment: *This work was financially supported by the Bulgarian National Science Fund through KP-06-OPR 04/5 project "Innovative hybrid supercapacitors as a challenge for efficient, safe and environmentally energy storage". Research equipment of distributed research infrastructure INFRAMAT (part of Bulgarian National roadmap for research infrastructures) supported by Bulgarian Ministry of Education and Science under contract D01-155/28.08.2018 was used in this investigation.*

REFERENCES

1. Lu Wang, Y. Han., X. Feng, J. Zhou, P. Qi, Bo Wang, *Coord. Chem. Rev.*, **307,** 361 (2016).
2. C. Zhao, W. Zheng, *Front. Energy Res.*, **3**, 1 (2015).
3. T. Cottineau, M. Toupin, T. Delahaye, T. Brousse, D. Bélanger, *Appl. Phys. A*, **82,** 599 (2006).
4. J. Chen, L. Xu, W. Li, X. Gou, *Adv. Mater.*, **17,** 582 (2005).
5. W., Zhang Wu X., J. Hu, Y. Guo, L.Wan, *Adv. Funct. Mater.*, **18**, 3941 (2008).
6. D. Cericola, R. Kötz, *Electrochim. Acta*, **72**, 1 (2012).
7. S. Veleva, A. Stoyanova, R. Raicheff, D. Kovacheva, M. Mladenov, *J. Progr. Res. Chem.*, **4**, 179 (2017).
8. B. E. Conway, *Electrochemical Supercapacitors*, Springer Science+Business Media New York 1999
9. A. Lasia, Electrochemical Impedance Spectroscopy and its Applications, Springer Science+Business Media New York 2014
10. P. L. Taberna, P. Simon, and J. F. Fauvarque, *J. Electrochem. Soc.*, **150**, A292 (2003)
11. R. Negroiu, P. Svasta, C. Ionescu, A. Vasile, 1st PCNS Passive Components Networking Days, 12-15th Sep 2017, Brno, Czech Republic, paper 3.2. Supercapacitors Session, PCNS2017 Proceedings Pg.56-62
12. M. Stoller, R. Ruoff, *Energy Environ. Sci.*, **3**, 1294 (2010).
13. M. Gaberscek, J. Moskon, B. Erjavec, R. Dominko, J. Jamnik, *Electrochem. Solid-State Lett.*, **11** A170 (2008).
14. D. Gruet, B Delobel, D. Sicsic, I. Lucas, V. Vivier, *Electrochim. Acta*, , **295**, 787 (2019).
15. F. Beguin, E. Frackowiak, Supercapacitors: Materials, Systems, and Applications, John Wiley &Sons., 2013.